Additive manufacturing of functional polymer-based composite with enhanced mechanoluminescence (ZnS:Mn) performance

Article *in* Journal of Composite Materials · March 2020

DOI: 10.1177/0021998320911975

CITATIONS
4

READS
149

4 authors:

Tawakalt Mayowa Akintola
Florida A&M University
10 PUBLICATIONS **27** CITATIONS
SEE PROFILE

Phong Tran Hoang
Florida State University
22 PUBLICATIONS **894** CITATIONS
SEE PROFILE

Charissa Lucien
Florida A&M University
2 PUBLICATIONS **4** CITATIONS
SEE PROFILE

Tarik J. Dickens
Florida A&M University-Florida State University College of Engineering
68 PUBLICATIONS **1,276** CITATIONS
SEE PROFILE

Article

JOURNAL OF COMPOSITE MATERIALS

Journal of Composite Materials
2020, Vol. 54(22) 3181–3188

DOI: 10.1177/0021998320911975
journals.sagepub.com/home/jcm
SAGE

Additive manufacturing of functional polymer-based composite with enhanced mechanoluminescence (ZnS:Mn) performance

Tawakalt Mayowa Akintola[1,2], Phong Tran[1,2], Charissa Lucien[1,2] and Tarik Dickens[1,2]

Abstract

Triboluminescence (TL) is a phenomenon of light emission induced by impact, stress, fracture, or an applied mechanical force. This phenomenon can be used to detect, evaluate, and predict mechanical failures in composites. In this report, we utilized manganese-doped zinc-sulphide (ZnS: Mn) and Polystyrene (PS) composite to fabricate a TL functional part via additive manufacturing. The morphology of the particles inside the polymer matrix were studied using scanning electron microscopy and micro CT scan. Thermoanalytical techniques such as differential scanning calorimetry (DSC) and thermogravimetric analysis (TGA) were carried out to evaluate the thermal transitions and degradation of the composites. The mechanoluminescence performance of the printed samples is evaluated by three-point flexural test and observed to depend on processing conditions that can be utilized to achieve a strong light signal at different mechanical loads. The polymer composite fabrication and processing reduced particle size, enhanced particle dispersion, and altered the mechanical properties of the polymer to help increase the mechanoluminescence response up to 10 times in the 3D printed parts. The unique mechanoluminescence properties of 3D printed luminescent composite have great potential for structural monitoring applications.

Keywords

Additive manufacturing, polymer, manganese-doped zinc-sulphide, polymer-matrix composite, triboluminescence, mechanoluminescence

Introduction

Triboluminescence/mechanoluminescence (TL/ML) is the emission of light as a result of inducing a mechanical load on centro-symmetric and non-symmetric materials.[1] Luminescent materials have attracted various research groups for applications in structural monitoring systems with advanced detection capabilities.[2,3] Xu et al.[4,5] developed a mechanical stress sensor by creating an artificial skin through the fabrication of a thin ML piezoelectric film, and Chandra et al.[6] studied the deformation of elastic ML of ZnS: Mn nanoparticles with an increase in luminescent intensity over time.

Dickens et al.[7] also reported on the micro-emission of triboluminescent concentrated composites and their evaluation at the onset of damage, crack propagation for structural damages, and sensing applications with emission occuring below its critical composite fracture energy.[2,8] Additive manufacturing (AM) as an advanced technology has been used to manufacture multi-materials[9–12] and multifunctional parts[13–16] with intricate and tailorable geometry.[17–19] A wide range of applications in additive manufacturing have been reported. Recently, Leigh et al.[20] demonstrated use of a low-cost 3D printer to produce a variety of functional electronic sensors. Also, Kennedy et al.[17] introduced a non-destructive and anti-counterfeiting method by embedding engineered nanomaterials into features of 3D printed parts to quantify a chemical signature profile. Marga et al.[21] used bioprinting-based technology

[1]Department of Industrial and Manufacturing Engineering, FAMU-FSU College of Engineering, USA
[2]High-Performance Materials Institute, USA

Corresponding author:
Tarik Dickens, FAMU-FSU College of Engineering, 2525 Pottsdamer Street, Tallahassee, FL 32310-6046, USA.
Email: dickens@eng.famu.fsu.edu

to fabricate 3D tissue and organ structure with complexity for cell proliferation. As 3D printing continues to gain interest in electronics,[20,22] ceramics materials[23,24] and biomaterials[21,25] the need for a method to monitor structural health and detect damage of the printed parts is essential.

In this work, we utilized Mn-doped ZnS as TL materials due to their intense mechanoluminescence properties, and polystyrene (PS) for the fabrication of the TL-PS functional parts via additive manufacturing. We discovered that by reducing the crystal size and polymer chains through multiple processing cycles, the following results were observed: (i) the distribution of crystals in the matrix could be improved by enhancing the TL-PS interface; (ii) an increase the mechanical properties of the composite; and (iii) an increase in the limunescent response up to 10 times – which allowed us to achieve printed samples with sensitive mechanoluminescence responses at different mechanical load levels.

Experimental work

Sample preparation

The ZnS: Mn particles (5–20 μm) were obtained from Phosphor Technologies, and the PS pellets (M_w ~35,000) were purchased from Sigma-Aldrich. The PS pellets were dried in an oven at 50 °C overnight and ground to a coarse powder before adding ZnS: Mn at 40% wt. The mixture of PS and ZnS: Mn (TL) was processed using the Haake™ Rheomex Twin Screw Extruder at 290 °C and extruded at 40 r/min speed through a die of 2.85 mm diameter. The TL-PS composite filament was cooled down and collected on a spool. The filament was then broken down into fine particles using a blender and re-extruded to attain samples with multiple extrusion and processing conditions (single, double, and triple extrusion). By controlling the extrusion speed, filaments with diameters of 2.85 mm and 1.5 mm were achieved for printing and testing, respectively.

The TL-PS filament was used as feedstock to print beams (55 × 5 × 10 mm) utilizing a fused filament fabrication (FFF) 3D printer (Lulzbot Taz 6) for three-point flexure testing on mechanical testing system. For all the prints, the temperature of the nozzle (0.5 mm) and the printing bed were set at 240 °C and 110 °C respectively.

Sample characterization

The morphologies of extruded filament at different processing conditions were evaluated using a Scanning Electron Microscope (SEM, JEOL 7400) at 5 kV. A high-resolution micro-computed tomography system (μ-CT Lab HX, Rigaku) was used to study the dispersion of TL particles within the second extruded TL-PS samples. Imaging was performed at a voxel size 2.13 μm with a source potential pf 90 kV and tube current of 88 μA. Each scan consisted of 1200 projections with the samples being rotated in steps about its longitudinal axis. The scanning time used a total of 2.5 h per specimen, and once the scanning was completed, the 3D dataset was then reconstructed using come beam approximation.

The transition temperature and thermal stability of TL-PS composite were determined using a Differential Scanning Calorimeter (DSC Q100, TA Instrument) set to equilibrate at 25 °C, hold isothermally for 10 min and ramp at 10 °C/min to 280 °C. The Thermogravimetric Analyzer (TGA Q50, TA Instrument) was established to ramp at 20 °C/min to 70 °C, hold isothermally for 10 min and ramp at 10 °C/min to 600 °C under nitrogen.

iNano Indentation System (Nanomechanics, Inc. Tencor, USA) was used to assess the mechanical properties of the PS and TL-PS filaments. The experimentation conducted at a continuous stiffness measurement performed 30 indents on the specimen, with 2.4 mN load and 810 μm depth, according to ISO 14577 standard.[26] Due to the irregular and small size of the composite, the sample was encapsulated in an epoxy (Epon Resin862) and cured. The cured composite samples were cut, and the surfaces were carefully polished, smoothened, and flattened for nanoindentation. Dynamic Mechanical Analysis (DMA Q800, TA Instruments) was used for the evaluation of the mechanical performance of the extruded filaments, according to ASTM D3379[27] Standard Test Method. All samples (diameter of 1.5 mm) were strained at 2%/min at a gauge length of 10 mm at room temperature.

Finally, the mechanoluminescence response of TL-PS composite printed parts was the study by conducting a flexural test on the different processing conditions. In brief, TL composite 3D printed beams were tested under three-point flexure (MTS insight) with a sample length of 50 mm and a cross-head speed of 2.5 mm/min according to ASTM D790[28] three-point flex. A Photomultiplier Tube (PMT, Hamamatsu H10722) was utilized to capture the illumination when the load was applied onto the samples. The electrical signal output that correlated to the light intensity was then recorded from the PMT using a USB-6210 DAQ (National Instruments). A constant load was applied on to 0.5 mm notched samples, and load–displacement plots were recorded as a function of time.

Experimental results and discussions

Morphology study of TL composites

The dispersion and the arrangement of functional particulates were examined under optical microscope,

SEM and μ–*CT*. Figure 1(a) shows the photographic images of the composite under UV light at 250 × magnification, and there are many ZnS crystals with the size of ZnS crystals is ~2–20 μm can be observed in the TL-PS composite. The shape features of these filler crystals become virtually undetectable on the surface of both the double and triple extruded samples (Figure 1(b) and (c)). The same observation of particle size change and better particle distribution can be seen in SEM images (Figure 1(d) and (e)) due to the grinding and blending of the composite before carrying out the successive double and triple strand processing routes. Three-dimensional reconstructed and cross-sectional μ–*CT* scan images (Figure 1(g) and (i)) display the uniform dispersion of TL particles in the PS matrix of the third extruded sample. The particle size varies from 1 to 20 μm with the majority of the particles with a size of less than 3 μm.

Thermal and structural analyses (TGA and DSC) of TL composite

The thermal stability and the weight percentage of the PS and TL-PS composite was analyzed using TGA with the generated thermogravimetric curves presented in Figure 2(a). The PS and TL-PS composite remained intact up until 300 °C. However, after that temperature the pristine PS decomposed rapidly without char yield

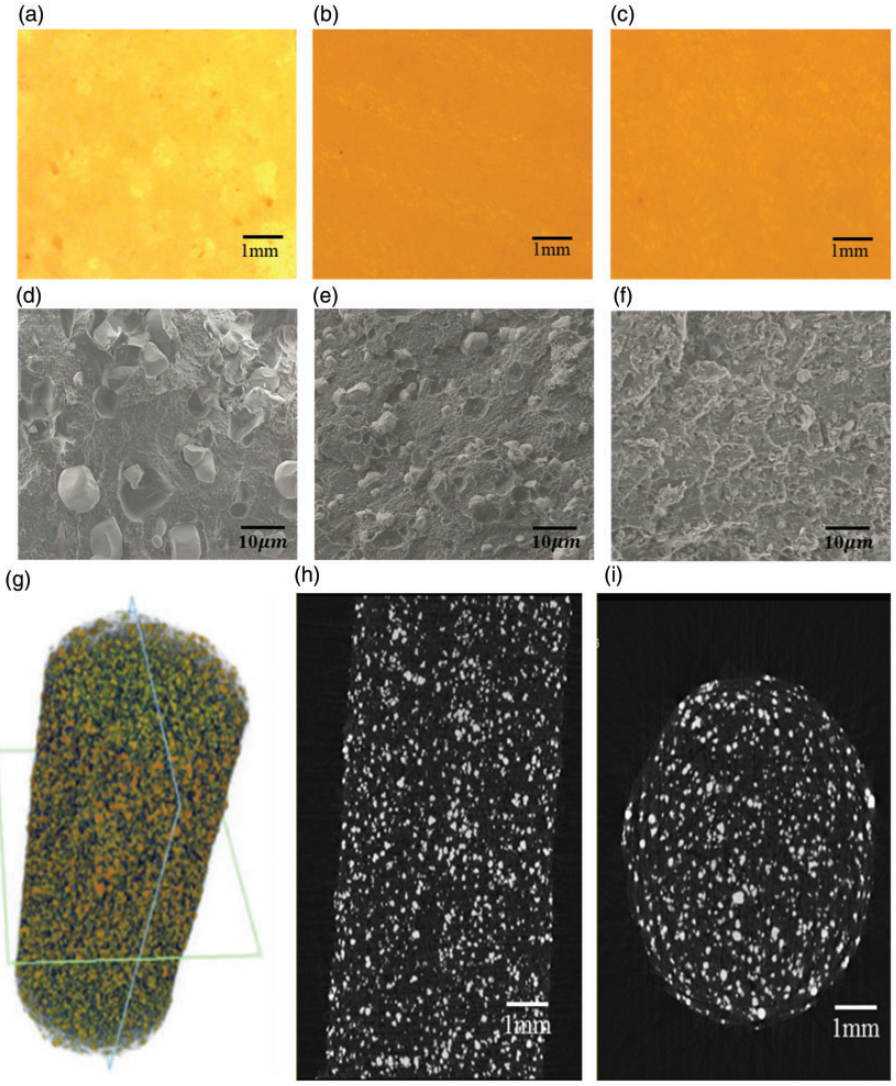

Figure 1. SEM images of (a) as-received ZnS-Mn (b) Single (c) double and (d) triple extruded TL-PS composite filament. Scale bar is 10 μm. Surface images at 250 × magnification under UV light before indentation indicating particle inclusion of TL-PS (e) single, (f) double, and (g) triple filaments processing, respectively. (g) 3D reconstructed images of μ–CT scan and (h, i) cross-sectional images of the third extruded sample.

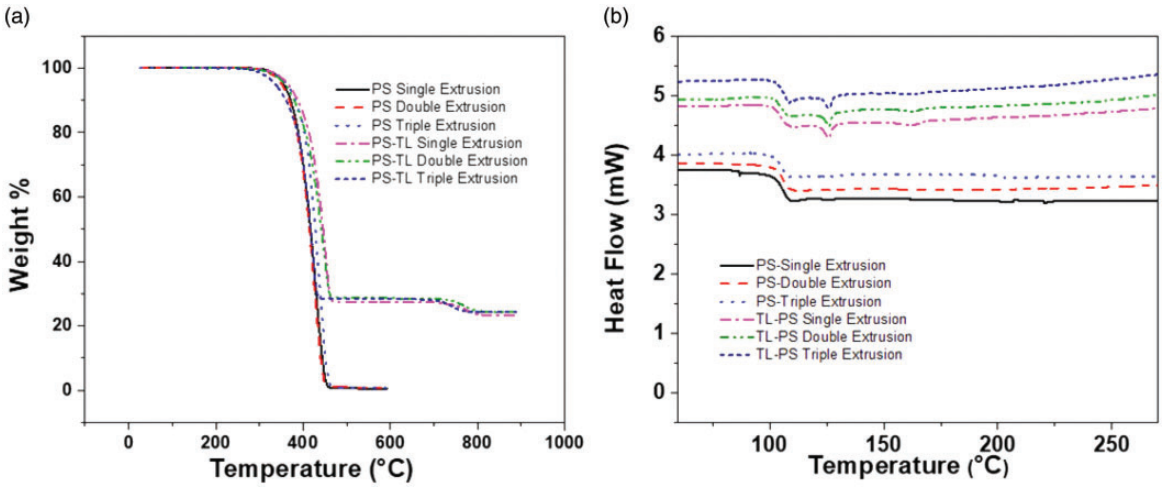

Figure 2. (a) TGA and (b) DSC results on PS and TL composite filament using three extrusion processes.

at the onset of 300–457 °C while the TL-PS composites demonstrated an onset around 304–464 °C. The initial weight decrease on both types of samples could be ascribed to the decomposition of PS. Polymers are reported to degrade during the thermal processing under high temperature which results in the reduction of molecular weight affecting the final material property.[29] The inclusion of the TL fillers alters the morphology due to random main-chain reaction and molecular mobility upon melt processing. This led to an improvement in thermal stability of the TL-PS composites compared to the pristine PS structure. Simultaneously, the ZnS particles have a significant depolymerization effect of suppressing molecular chain transfer reactions, and redistribution to slow down the decomposition process of the polystyrene polymer, which assists composites with the high thermal stability.[29] The weight loss of TL-PS composites slightly varied between processing conditions around 70 wt% of the initial weight. This indicates a concentration of 30% of ZnS in the TL-PS composite. The TL-PS composite show an additional weight loss over 750 °C due to the thermal dissociation and sublimation of the zinc sulphide facilitated by the nitrogen flow.[30,31] The TL filler weight percentage in the TL-PS composite is about 31.5 wt% and the residual mass percentage of the TL-PS composites at 900 °C is about 23.6 wt%.

Differential calorimetry scanning (DSC) curve (Figure 2(b)) for pristine PS obtained from different processing conditions shows the glass transition (T_g) occurred at almost the same temperature for both the PS and TL-PS samples. During the testing, only a slight reduction of T_g was noticed which may be due to the degradation of the polymer throughout the different processing cycles. This observation is related to the reorganization of the amorphous domain into crystalline due to increasing molecular mobility upon increasing temperature.[29] As shown in the DSC graph (Figure 2(b)), the first endothermic peak observed in the PS and the TL-PS composite is around 125 °C. This peak may be attributed to the evaporation and slow crystallization rate in the TL-PS composite. The second peak observed in the TL-PS composite is due to presence of the lattice deformation of ZnS crystals.[3,30,31]

The addition of ZnS particles and the multiple processing conditions appear to have no apparent effect on the glass transition temperature in the TL-PS composite, instead it reduces the heat capacity as seen by the lesser second peak. In terms of 3D printability, since there is no change in the TL-PS composite's glass transition temperature (104 °C), a printing temperature of 240 °C could be used for the pristine PS and TL-PS composite.

Micro-mechanical properties

To further examine the mechanical properties and the particulate uniformity of the samples, 30 indentation tests were conducted on different locations on both the PS and TL-PS composite with the single, double, and triple processing steps. The indents were made using the advanced dynamic modulus and hardness method according to the nanoindentation procedures applied to the composites, with a set maximum load and depth and constant Poisson's ratio approximately at 2.4 mN, 810 nm, and $\upsilon = 0.3$, respectively.[32,33] The method works by measuring the indentation depth and contact stiffness through a specified load applied to the specimen. The measured values are then converted to hardness through the Oliver-Pharr indentation model.[34]

The average local hardness (H) results with the different PS and TL-PS composite processing are shown

in Figure 3. The experimental data show that with the increase of extruded cycles, the pristine PS hardness decreased from 0.34 to 0.05 GPa. In contrast, the TL-PS composite sample showed an initial decrease from 0.28 to 0.18 GPa followed by a 3 × increase to 0.53 GPA for the triple extruded sample.

The PS polymer, when processed at a continuous extrusion and grinding, undergoes chain-session.[29,35] This change is the cause for the hardness degradation in the pristine PS samples. The significant increases in hardness for the triple processed state of the TL-PS composite can be attributed to two factors (i) the hardness of the perforated ZnS crystals particles, which are known to have higher hardness values than PS,[36] and (ii) the mixing effect of small particles which leads to a better dispersion of the crystal within the composite matrix. However, the similar hardness and trend of the first two processed TL inclusion and TL-PS samples, indicated that the TL particulates were not dispersed well within the composite matrix.

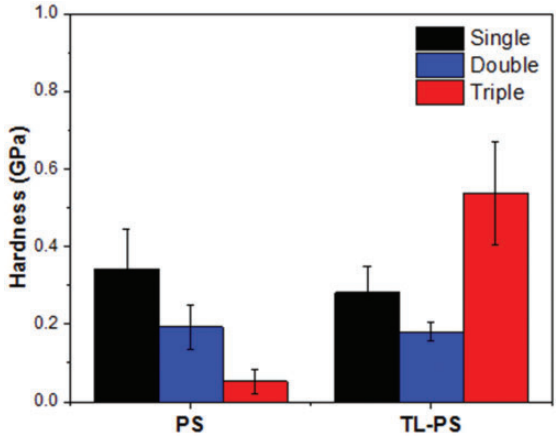

Figure 3. Nanoindentation hardness results of PS and TL-PS single, double, and triple extruded samples.

The number of processing cycles was observed to have the opposite effect on the mechanical properties of the pristine PS and TL-PS composites, as shown in Figure 4. The more processing cycles the PS samples underwent, the more brittle the samples were as the processing shortened which changes the mobility chain of the polymer (chain session).[29]

Meanwhile, when ZnS particles were introduced into the matrix, the TL-PS composite samples show a reducing trend of ductileness with the increasing of processing cycles. This can be explained by the size reduction of ZnS particles caused by mechanical processing, which in turn may improve the particle distribution, interfacial bonding, and stress transfer from the matrix. Additionally, the stiffness and strength of TL-PS composite samples were shown to be higher than PS. The addition of ZnS particles makes the TL-PS composite stronger and more brittle since it may help to prevent crack propagation and diminishes the alignment of polymer chains when subjected to a tensile force.[29]

Mechanoluminescence fracture testing

Mechanoluminescence (ML) fracture tests were carried out to understand the relationship between the applied stress and TL emission, as well as the effect of the

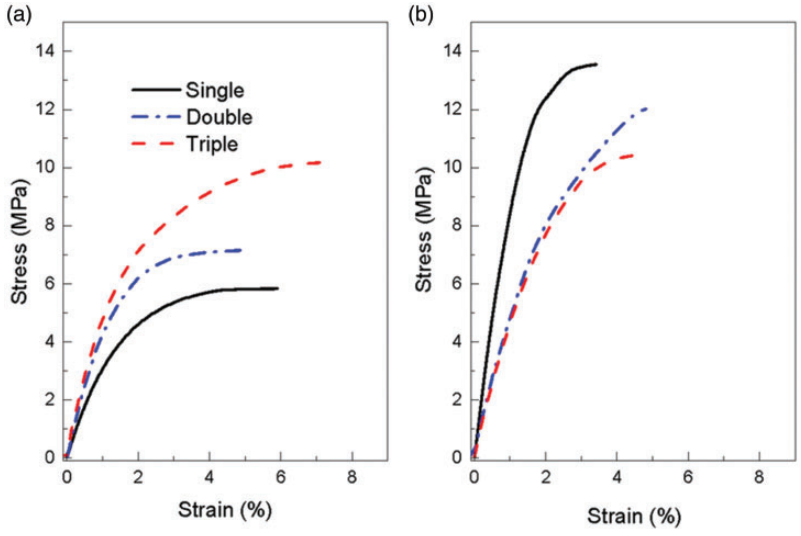

Figure 4. Stress–strain curve of (a) PS and (b) TL-PS composite at different processing conditions.

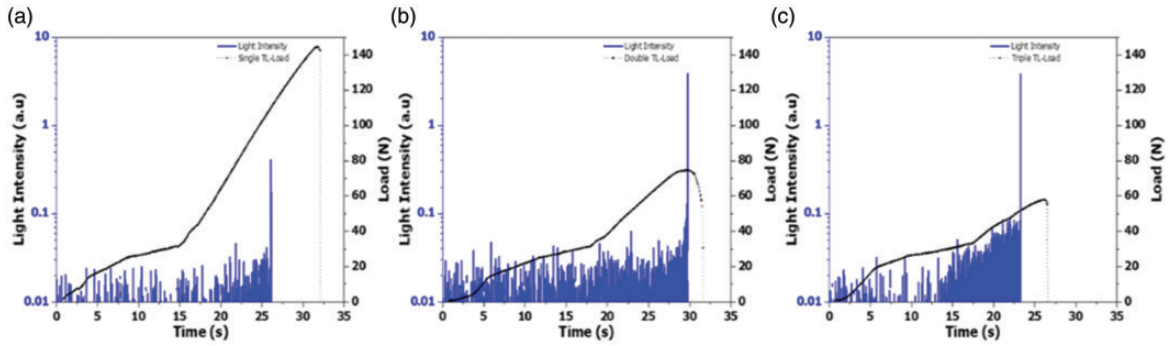

Figure 5. Schematic test setup for three points bending on TL beam samples using MTS insight and comparison of the TL signal emission plot in Load mode for (a) single (b) double (c) triple TL composite beam concerning the time.

structural alteration of the 3D printed TL-PS composite. As shown in Figure 5, the TL emission occurred when the flexural load in the fracture test samples was transferred from the polymer matrix to the crystals. This induced stress on the neighboring crystals. Figure 5(a) to (c) is identically scaled to observe the difference in the excitation peaks and the loading constraint of the processed functional material.

It can be observed that the 3D printed TL-PS composite samples exhibited a significant change in emission levels, across Figure 5(a) to (c). This means that the change depended upon the mechanical loads where the excitation responses occurred which directly related to the processing cycles. The failure point of the single extruded samples was at 140 N, which is approximately 1.87 and 2.88 times higher than the double and triple extruded samples, respectively. This is due to the increasing brittleness of the processed TL-PS composite samples.

Meanwhile, the intensity of the mechanoluminescent signal of the TL-PS composite samples improved, as the highest light intensity was observed at 0.41, 3.91, and 3.82 (a.u) for the single, double, and triple processing, respectively. Compared to the single extrusion, even with the smaller loads, the light intensity of the double and triple extrusion was approximately one order of magnitude larger. The smaller crystal size is expected to have better distribution and a larger surface area within the matrix. This may improve the load transfer as the mechanical load on the small size crystal is more pronounced. This is a significant observation over previous studies where the size effect has been looked at from a synthesis point of view[37] or based on an excited population potential.[38] The effect of processing on the polymer matrix shortens the polymer chain, increases the brittleness of the polymer, which releases more energy onto the crystal, and results in a better mechanoluminescence response found in double and triple extruded samples. These results indicate the uniqueness of the processing cycles with the inclusion of ZnS crystals in the composite, which enhance the mechanoluminescent performance.

Conclusions

TL-PS composite filament was manufactured to fabricate functional parts using the filament additive manufacturing technique. The thermoplastic composite filaments were found to be thermally stable and functionally non-destructive, despite multi-processing cycles and inclusion of TL particulate materials. Additionally, it was discovered that the processing conditions and ZnS particle inclusion in the polymer-matrix composites played a vital role in mechanoluminescence response of the printed parts. Nanoindentation results determined the composite's mechanical properties as the triple processed extruded sample exhibited the highest hardness 0.53 GPa, while the polymer chain is thermally unstable and degrades its hardness due to processing. Also, the process conditions control the particle size and matrix hardness, which justify the mechanical behavior in the nanocomposite. The better distribution of small size TL crystals into the modified polymer matrix has been observed, and corroborated through SEM and microCT imaging, to significantly increase the light intensity of the printed parts when they were subjected to the mechanical loading. At a different level of mechanical load or the structural capacity, the light intensity of samples with double and triple extrusion cycles was found to be 10 times larger than the initially processed extrusion samples. By controlling the properties of the polymer matrix and the TL crystals, we can tune the sensitivity and working range of 3D printed parts. The results suggest that TL emission may reveal path crack propagation[39] since the emission is bound to occur upon the failure of ZnS crystals in the matrix. This research would provide a novel approach for the fabrication of embedded sensors for structural health monitoring of parts produced by additive manufacturing.

Acknowledgements

The authors wish to thank NSF for the funding "NSF CREST #1735968 and RISE #1646897", High-Performance Materials Institute for the use of the facility, Madhuparna Roy and Jolie Breaux Frketic, for their contribution toward the completion of this research. They also thank the Rigaku Americas Corporation application team as well, namely Aya Takase, for their contribution of CT images.

Declaration of Conflicting Interests

The author(s) declared no potential conflicts of interest with respect to the research, authorship, and/or publication of this article.

Funding

The author(s) disclosed receipt of the following financial support for the research, authorship, and/or publication of this article: This research was supported through NSF-CREST RISE (proposal no. 1646897).

ORCID iD

Tarik Dickens https://orcid.org/0000-0002-7046-3508

References

1. Persits N, Aharoni A and Tur M. Quantitative characterization of ZnS:Mn embedded polyurethane optical emission in three mechanoluminescent regimes. *J Lumin* 2017; 181: 467–476.
2. Olawale DO, Dickens T, Sullivan WG, et al. Progress in triboluminescence-based smart optical sensor system. *J Lumin* 2011; 131: 1407–1418.
3. Murugadoss G. Synthesis and characterization of transition metals doped ZnO nanorods. *J Mater Sci Technol* 2012; 28: 587–593.
4. Xu CN, Watanabe T, Akiyama M, et al. Artificial skin to sense mechanical stress by visible light emission. *Appl Phys Lett* 1999; 74: 1236–1238.
5. Xu CN, Watanabe T, Akiyama M, et al. Preparation and characteristics of highly triboluminescent ZnS film. *Mater Res Bull* 1999; 34: 1491–1500.
6. Chandra BP, Xu CN, Yamada H, et al. Luminescence induced by elastic deformation of ZnS:Mn nanoparticles. *J Lumin* 2010; 130: 442–450.
7. Dickens TJ, Breaux J, Olawale DO, et al. Effects of ZnS:Mn concentrated vinyl ester matrices under flexural loading on the triboluminescent yield. *J Lumin* 2012; 132: 1714–1719.
8. Dickens TJ and Okoli OI. Enabling damage detection: manufacturing composite laminates doped with dispersed triboluminescent materials. *J Reinf Plast Compos* 2011; 30: 1869–1876.
9. Gnanasekaran K, Heijmans T, van Bennekom S, et al. 3D printing of CNT- and graphene-based conductive polymer nanocomposites by fused deposition modeling. *Appl Mater Today* 2017; 9: 21–28.
10. Lee J-Y, An J and Chua CK. Fundamentals and applications of 3D printing for novel materials. *Appl Mater Today* 2017; 7: 120–133.
11. Wang X, Jiang M, Zhou Z, et al. 3D printing of polymer matrix composites: a review and prospective. *Compos Part B Eng* 2017; 110: 442–458.
12. Nguyen N, Melamed E, Park JG, et al. Direct printing of thermal management device using low-cost composite ink. *Macromol Mater Eng* 2017; 302: 1700135.
13. Luong DX, Subramanian AK, Silva GAL, et al. Laminated object manufacturing of 3D-printed laser-induced graphene foams. *Adv Mater* 2018; 30: 1707416.
14. Chua CK and Leong KF. *3D Printing and additive manufacturing: principles and applications (with Companion Media Pack). Fourth Edition of Rapid Prototyping*. Singapore: World Scientific Publishing Company, 2014.
15. Bailey C, Stoyanov S, Tilford T, et al. Multi-physics models and condition-based monitoring for 3D-Printing of electronic packages. In: *2017 18th International conference on thermal, mechanical and multi-physics simulation and experiments in microelectronics and microsystems (EuroSimE)*, 2017, pp. 1–8. US: Institute of Electrical and Electronics Engineers (IEEE) Publishing.
16. Jiao L, Chua ZY, Moon SK, et al. Laser-induced graphene on additive manufacturing parts. *Nanomaterials* 2019; 9: 90.
17. Kennedy ZC, Stephenson DE, Christ JF, et al. Enhanced anti-counterfeiting measures for additive manufacturing: coupling lanthanide nanomaterial chemical signatures with blockchain technology. *J Mater Chem C* 2017; 5: 9570–9578.
18. Oxman N. Variable property rapid prototyping. *Virtual Phys Prototyp* 2011; 6: 3–31.
19. Beidaghi M and Gogotsi Y. Capacitive energy storage in micro-scale devices: recent advances in design and fabrication of micro-supercapacitors. *Energy Environ Sci* 2014; 7: 867–884.
20. Leigh SJ, Bradley RJ, Purssell CP, et al. A simple, low-cost conductive composite material for 3D printing of electronic sensors. *PLOS One* 2012; 7: e49365.
21. Marga F, Jakab K, Khatiwala C, et al. Toward engineering functional organ modules by additive manufacturing. *Biofabrication* 2012; 4: 022001.
22. Sarobol P, Cook A, Clem PG, et al. Additive manufacturing of hybrid circuits. *Annu Rev Mater Res* 2016; 46: 41–62.
23. Zocca A, Colombo P, Gomes CM, et al. Additive manufacturing of ceramics: issues, potentialities, and opportunities. *J Am Ceram Soc* 2015; 98: 1983–2001.
24. Eckel ZC, Zhou C, Martin JH, et al. Additive manufacturing of polymer-derived ceramics. *Science* 2016; 351: 58–62.
25. Huiling Loo A, Kiang Chua C and Pumera M. DNA biosensing with 3D printing technology. *Analyst* 2017; 142: 279–283.
26. Ebenstein DM and Wahl KJ. A comparison of JKR-based methods to analyze quasi-static and dynamic indentation force curves. *J Colloid Interface Sci* 2006; 298: 652–662.

27. Swaminathan G and Shivakumar K. A re-examination of DMA testing of polymer matrix composites. *J Reinf Plast Compos* 2009; 28: 979–994.
28. Hurst JB, Hong WS, Gambone ML, et al. ASTM single fiber room temperature test standard development. In: *ASME 1998 International Gas Turbine and Aeroengine Congress and Exhibition*. American Society of Mechanical Engineers Digital Collection, 1998; V005T13A017.
29. Signori F, Coltelli M-B and Bronco S. Thermal degradation of poly (lactic acid)(PLA) and poly (butylene adipate-co-terephthalate)(PBAT) and their blends upon melt processing. *Polym Degrad Stab* 2009; 94: 74–82.
30. Cadiş AI, Tomşa AR, Bica E, et al. Preparation and characterization of manganese doped zinc sulphide nanocrystalline powders with luminescent properties, https://scholar.googleusercontent.com/scholar?q = cache:_EY2hYWMpdkJ:scholar.google.com/ + PREPARATION + AND + CHARACTERIZATION + OF + MANGANESE + DOPED + ZINC + SULPHIDE + NANOCRYSTALLINE + POWDERS + WITH + LUMINESCENT + PROPERTIES + &hl = en&as_sdt = 1,10 (accessed 31 January 2020).
31. Mu J, Gu D and Xu Z. Effect of annealing on the structural and optical properties of non-coated and silica-coated ZnS:Mn nanoparticles. *Mater Res Bull* 2005; 40: 2198–2204.
32. Chen W, Huang G, Lu H, et al. Utilizing nanofabrication to construct strong, luminescent materials. *Nanotechnology* 2006; 17: 2595–2601.
33. Yang C-H, Lee C-Y, Huang B-C, et al. Nanoindentation study of single-crystalline and (101)-oriented nanotwinned Cu. *ECS J Solid State Sci Technol* 2019; 8: P363–P369.
34. Oliver WC and Pharr GM. Measurement of hardness and elastic modulus by instrumented indentation: advances in understanding and refinements to methodology. *J Mater Res* 2004; 19: 3–20.
35. Xiao M, Sun L, Liu J, et al. Synthesis and properties of polystyrene/graphite nanocomposites. *Polymer* 2002; 43: 2245–2248.
36. Walton AJ. Triboluminescence. *Adv Phys* 1977; 26: 887–948.
37. Bhargava RN, Gallagher D, Hong X, et al. Optical properties of manganese-doped nanocrystals of ZnS. *Phys Rev Lett* 1994; 72: 416–419.
38. Chandra BP. Mechanoluminescence. In: Vij DR (ed) *Luminescence of solids*. Boston: Springer US, pp. 361–389.
39. Joshi K, Mishra S, Campbell C, et al. Light emitting composite beams during matrix cracking. *J Compos Mater* 2017; 51: 4251–4260.